Neuroprotective upshot of isorhoifolin flavonoid of Gmelina asiatica for multitargeted approach in Alzheimer's disease: Exploration through in-silico studies

Komal Rajesh Andarghiske
Indian Institute of Technology, Banaras Hindu University
Bhanukiran Kancharla
Indian Institute of Technology, Banaras Hindu University
Hemalatha Siva
shemalatha.phe@itbhu.ac.in

Indian Institute of Technology, Banaras Hindu University

Research Article

Keywords: Alzheimer's disease, DFT, G. asiatica, molecular dynamics, isorhoifolin flavonoid, Multitargeted approach

Posted Date: October 9th, 2023

DOI: https://doi.org/10.21203/rs.3.rs-3408123/v1

Additional Declarations: No competing interests reported.

Abstract

Alzheimer's is a progressive neurodegenerative disease with amyloid-beta peptide deposition that impairs memory and cognitive decline. In previous reports, the plant *Gmelina asiatica* was reported to have anti-Alzheimer's disease (AD) activity. However, the responsible chemical constituents of *G. asiatica* for anti-Alzheimer's activity have not been explored. Therefore, the present study aimed to investigate hit compounds through an *in silico* approach. The reported phytoconstituents were initially screened through auto dock software. Then, the lead compound was further evaluated through molecular dynamic studies. Further hit compound isorhoifolin physicochemical and ADMET properties were analyzed. In docking studies, isorhoifolin showed the least binding energy and well resided at the active sites of AchE (-10.9 kcal/mol), BACE1 (-10.2 kcal/mol), GSK-3 (-9.7 kcal/mol), TACE1 (-9 kcal/mol). Further molecular dynamic simulation revealed that isorhoifolin is stable up to 200 ns. Furthermore, density functional theory (DFT) was analyzed using Gaussian software, where the quantum mechanics objective was focused. Besides, the physicochemical properties of isorhoifolin were studied, such as absorption, distribution, metabolism, excretion, and toxicity, through the pkcsm software. The study suggests isorhoifolin from the *Gmelina asiatica* plant may be responsible for anti-Alzheimer's activity, which may be considered for further investigation.

Introduction

Alzheimer's disease, affecting over 55 million adults worldwide, is a progressive neurodegenerative condition characterized by behavioral changes, cognitive impairment, and daily routine errors [1]. Factors contributing to the disease include acetylcholine insufficiency, beta-amyloid accumulation, and neurofibrillary tangle deposition [2]. Genetic factors, such as mutations in amyloid precursor protein genes, also play a role in the disease's pathogenesis, causing cognitive decline and brain tissue deterioration [3, 4]. FDA-approved drugs for Alzheimer's include donepezil, rivastigmine, galantamine, memantine, aducanumab, and lecanemab, but side effects limit effectiveness. New approaches include molecule inhibitors, immunotherapy, and Aβ blockers [5]

This study has four target proteins linked to Alzheimer's disease progression: AChE inhibitor, TACE, GSK-3, and BACE1 [6, 7]. AChE inhibitors are the most curative treatment where cholinesterase enzyme inhibition leads to cholinergic neuron augmentation [8]. TACE is a TNF-alpha-converting enzyme. Its level in the healthy brain is average but higher in AD patients [9, 10]. Inhibition in the level of TACE enzyme will help in the reduction of neuroinflammation.GSK-3 overexpression distinguishes AD patients' neurons from normal healthy individuals' brains [11]. It leads to tau protein phosphorylation, AD causes tau protein phosphorylation, and BACE1 is a schematic enzyme that cleaves APP at the β-site. Prevention of APP cleavage will reduce Aβ production in the brain prevents APP cleavage, reducing Aβ production in the brain [12].

Natural products, including phytoconstituents and antioxidants, have improved Alzheimer's disease (AD) treatment [13]. Ancient Egyptian, Indian, and Chinese cultures have used naturopathic medicine,

including phytotherapy from herbal plants. Although functionally tested, few have been clinically tested [14]. Secondary metabolites from plants like *Ginkgo biloba, Centella asiatica, Withania somnifera, Salvia officinalis Lepidummeyenii, Glycyrrhiza glabra*, and *Convolvulus pluricaulisand* have also been utilized [15].

In this study, we used *Gmelina asiatica* L (Verbenaceae), which is commonly known as Nilakkumil in Tamil and Gopabhandra in Sanskrit. The plant *Gmelina arborea* reported to have various pharmacological activities, especially nootropics, epilepsy, and other CNS disorders [16]. *Gmelina asiatica* and *Gmelina arabica* belong to the same genus and have similar phytochemical profiles [17]. The following phytoconstituents were reported from these plants, i.e., cycloolivil, spathulenol, nicotiflorin, gmelinol, quercetagetin, pinoresinol, sakuranetin, luteolin-7-glucuronide, poulownin and isorhoifolin which we considered for the current study (Fig. 1).

Results and Discussion

Molecular docking studies

Screening of phytochemicals by docking

Auto-dock software was used for the molecular docking studies [18]. Binding free energy and types of interactions are some of the essential parameters analyzed in the docking study. Table 1 represents each phytoconstituent's docking binding energy values with specific proteins. Among all constituents, isorhoifolin showed the least binding energy compared to the other phytochemicals in plant leaves.

Table 1
Binding energies of phytoconstituents with target protein receptors of AD.

Sr No	Phytoconstituents	6ZWE (AChE) [kcal/mol]	4FRJ (BACE-1) [kcal/mol]	1Q5K (GSK-3) [kcal/mol]	2OI0 (TACE) [kcal/mol]
1	Cycloolivil	-7.6	-7.4	-7.2	-7.5
2	Spathulenol	-7.9	-7.5	-7.5	-6.8
3	Nicotiflorin	-9.1	-9.9	-9	-8.5
4	Gmelinol	-9.3	-7.8	-7.8	-9.5
5	Quercetagetin	-9.3	-8.4	-8.5	-8.9
6	Pinoresinol	-9.4	-8.5	-8.5	-8
7	Sakuranetin	-9.7	-8.4	-8.5	-8.5
8	Luteolin-7-glucoronide	-9.9	-10.4	-9.6	-9.8
9	Poulownin	-10.8	-9.4	-8.8	-9.2
10	Isorhoifolin	-10.9	-10.2	-9.7	-9

Table 2
Interactions of target proteins with isorhoifolin

S. No.	Target protein	Types of bond interaction	Amino acid residues
1	4FRJ (BACE1)	Conventional hydrogen bond	ASN233, TRP76, GLN73, GLY230, ASP32, ARG235
		Alkyl	VAL332
		Vander Wall forces	THR232
2	6ZWE (AChE inhibitor)	Conventional hydrogen bond	PHE295, TYR341, TYR134
		Pi-Pi T shaped	PHE297, PHE338, TRP286
3	1Q5K (glycogen synthetase kinase GSK-3)	Conventional hydrogen bond	GLU185, VAL35
		Pi-Sigma	LEU189, CYS199, VAL70, ILE62
		Pi-Alkyl	LEU189
4	2OI0 (TNF-alpha converting enzyme)	Conventional hydrogen bond	GLN185, VAL135
		Pi-Sigma	VAL70, ILE62
		Pi-alkyl	LEU188, CYS199, VAL62

In the BACE1-isorhoifolin complex, the formation of conventional hydrogen bonds with oxygen and hydrogen of the phenyl ring with amino acid ASN233 and Vander Waals bonds with THR232, respectively, makes stable bond formation of the complex. Other than phenyl ring cyclohexyl and phenolic hydrogen with oxygen creating a hydrogen bond with amino acid residues of TRP76, ASP32 enhances the complex's stability. Alkyl bond formation between VAL332 of the amino acid residue and hydrogen of the oxy-cyclohexyl ring shows the saturation nature of the ligand isorhoifolin, which helps the ligand for the assembly of the complex (Fig. 2).

For the AChE inhibitor-isorhoifolin complex, there was a various nature of bond formation that helped the ligand form the anchored composite. Conventional and Vanderwalls bonds formed between isorhoifolin and amino acid residues TYR124 and GLY121, respectively (Fig. 2). Apart from these interactions, ketonic oxygen and phenolic hydrogen of isorhoifolin interact with the target protein's PHE295 and TYR341 amino acid residues, creating a hydrogen bond. TRP286 and PHE297 residues of AChE target protein (6ZWE) had pi-pi stacked T-shaped bond attraction with the phenolic ring and ketonic oxycyclohexyl ring of isorhoifolin, resulting in sturdy attributes of complex (Table 2).

The GSK3-isorhoifolin conglomerate had profuse bond intricacy, where there was an unfavorable donor-donor bump between cyclohexyl and phenolic hydrogen of isorhoifolin with CYS183 and TYR138 amino

acid residues of target protein GSK-3. Besides these conventional bonds between oxy cyclohexyl and phenolic hydrogen with VAL135, GLN185 amino acid residues of the target protein compensate for the bump of donor-donor. Pi-pi sigma interactions are seen between amino acid residues VAL70 and ILE62 with quinolic and phenolic hydrogen of ligand (Fig. 2). The last pi-sigma nature is also seen in the complex where LEU188 and CYS199 amino acid residues are fused with phenolic and quinolinic hydrogen of ligand.

TACE target protein (2OI0) with isorhoifolin ligand network conventional hydrogen, van der Walls, amide-pie stacked, pi-alkyl, and one bump glimpsed. Amino acid residues for conventional and Vander walls hydrogen bond involved are ASW447, GLU406, and PRO437 with oxygen, hydrogen of phenol and quinol, and cyclohexyl carbon, respectively. Saturating nature bonds like amide-pi stacked and pi-alkyl also contribute to the complex's higher binding energy than the other phytoconstituents of plants. TYR433 of residues with phenyl ring LEU401, VAL434 residues with phenolic hydrogen, and VAL402, ALA439, and LEU348 of residues with quinolinic hydrogen of isorhoifolin had the solid interaction (Fig. 2).

The above synergy of isorhoifolin with the target protein is responsible for its high binding energy, contrary to the other phytochemicals of the plant. Hence, we used isorhoifolin phytoconstituent for further molecular dynamics and DFT calculation. The most stable complex for the MD simulation analysis was selected based on the binding energy of the complex. Table 1 shows that BACE1-isorhoifolin and AChE inhibitor-isorhoifolin had the highest binding energy, -10.2 and – 10.9, respectively. These two complexes were further analyzed for MD studies.

Docking validation

The perceptible illustration of the correlation between the contender of test precision and vulnerability was computed throughout the ROC curves. The ROC curve generation was initiated by delineating the rate of authentic positives proportionate to the percentage of false positives commensurate to the percentage of true negatives. The outlined ROC curve design was availed to substantiate the chosen phytoconstituents for molecular docking studies so that designated compounds should be from functional ligands rather than idle ligands (decoys). Furthermore, the delineated pattern differentiated the active ligands from the best-in-class phytoconstituents in the chosen database. The values 0.7788462 and 0.708333 are discernible areas under the curve, and an enrichment factor was discovered in the top 1% at 3.25 and 3.05 as well grounded (Fig. 3). The ROC curve is the correlation between responsiveness and specificity. It corresponds to the presentations of actual positive and false positive fractions on the y-axis and x-axis. The values 0.7788462 and 0.708333 are good areas under the ROC, representing that the docking gimmick played a significantly specific and accurate role in docking with target receptor proteins 4FRJ and 6ZWE, respectively, with isorhoifolin.

Molecular dynamics studies

A RESPA integrator was employed to amalgamate all the frameworks of the dynamic environment of interlinkage and component firmness. Docking concordats are usually expeditious and coarse-grained;

nevertheless, docking scantiness protein pliability can mediate with the reliability of the concomitant target protein-ligand complexes. Therefore, a detailed molecular dynamics simulation methodology might ameliorate a preferable harmonizing with docking [19]. Substantially, MD is accustomed to gauging macromolecular and contingent variables based on conventional mechanics and by using Newton's analogy of motion to reckon the speed and locus of each atom of the contemplated organization. That means MD accomplishes a more rigorous vindication than docking studies. The study helps in the solvation investigation of molecules along with characteristics of the target protein and protein-ligand interlinkage, perhaps investigated through MD [20]. This study selected the most favoured constituents for further dynamics study based on binding energy and numbers with the type of interaction through molecular docking study. It was observed that isorhoifolin was the compound that had the highest binding energy and a good number of interactions as compared to other phytoconstituents of *G. asiatica*. Utilizing the best complexes and docking conformations found from Auto Dock, they were examined for plausible atomic characteristics within the solvent system [21]. For that purpose, complexes of BACE1-isorhoifilon and AChE inhibitor-isorhoifolin were further selected for dynamics study. Interchange allying protein along with ligand is conceivably elucidated by PL and LP proximity bar representations (Fig. 4A) for ligand fleck (Fig. 4B). The diagram manifests assorted peculiar interactions of the ligature in the company of amino acid residues of the target protein, additionally designated as hydrogen, hydrophobic, ionic bonds, and water aqueducts [22]. Two target protein-ligand complexes, BACE1-isorhoifolin and AChE inhibitor-isorhoifolin, were deliberated through MD simulations to inaugurate the steadiness of the complex. The comprehensive perusal of trajectories acquired from the MD run was scrutinized for target proteins BACE1, AChE inhibitor, and ligand isorhoifolin RMSD, RMSF, torsion portrayal, and hydrogen bonding [23].

The Fig. 4 bar illustration showed hydrogen bonding with amino acid residues GLY 32, TRP 36, PRE108, ARG235 for BACE1-isorhoifolin complex whereas for AChE inhibitor-isorhoifolin seemed to be THR95, GLU292, SER293. Ionic bonding with amino acid residues ASP32 & 298 for BACE1-isorhoifolin and AChE inhibitor-isorhoifolin complex was found to be with ALA204, ASN283. For hydrophobic interactions, residues involved were THR71 and ILE118 of the BACE1-isorhoifolin complex, whereas, in complex 6ZWE-isorhoifolin, these interactions are with amino acid residues of MET85, GLY122, GLU285, TYR337 & VAL340.

Protein RMSD outlines the gesticulation of divergent ligand atoms contemporary in the active site of the target protein receptor and anticipates the structural contour of the protein throughout MD. The consummate aberration in RMSD for most globose proteins is contemplated in the ambit of 1–4Å. RMSD of 4FRJ and 6ZWE come across protein mainstay RMSD of 1.8 Å & 2.8 Å, and for ligand, it was shown deviation of 1.5 Å & 1.8 Å.

In the ligand RMSD plot context, the Lig-fit port indicates a valued subordinate to the protein RMSD, prudent that the ligand is conscientiously disseminated to the commencing binding site and contrariwise. The orientation also proclaims that the ligand is well resided inside the binding site Fig. 5 (A) & (B). RMSF succor in prognosticating the structural rectitude of the target receptor protein-ligand

complex constituted by RMSF nomograms P-RMSF and L-RMSF. The P-RMSF delineates provincial transpose in the protein chain, forasmuch as L-RMSF Fig. 5 (C), (D), (E), and (F) chronicle commute in the orientation of ligand atoms. In the bargain, protein RMSF (P-RMSF) is acclimated to appraise the obligatory steadiness of the protein by distinguishing the fluctuation in the vertexes of the plot throughout the simulation. The standard P-RMSF was correspondingly considered 1.8 Å & 2.4Å for BACE1-Isorhoifolin & 6ZWE-Isorhoifolin complexes. The ligand RMSF exhibit for BACE1-isorhoifolin AChE inhibitor-isorhoifolin was discovered to be 6 Å and 3 Å, respectively.

Ligand contortion is a requisite parameter to scrutinize the energy dynamic obligation of ligand conclusive free energy, with the numerical signification of the malleable. The contour exchanges that each rotatable bond (RB) afforded by ligand molecule that encounters all over its MD miniature could be outlined from its ligand torsion silhouette. In Fig. 6, assorted rotatable bonds inside the ligand structure are colour-enciphered diversely and portrayed with a dial and bar plot intimated in colour to communicate to the corresponding bond. The phase of the bar plot constitutes the prospect of torsions as a corollary of angle, and the dial plot exhibits the torsional angle as it synchronizes and lengthens cochlearly toward the edge throughout the simulation. isorhoifolin expressed the occupation of four rotatable bonds in the middle of carbon atoms of phenyl aliphatic ring for a protein 4FRJ & 6ZWE complex.

Assets like hydrogen bonds necessitate consideration for developing novel advanced drugs that cause hydrogen bonding to have a consequential notable influence on drug exactitude, absorption, metabolism, etc., due to association in the ligand binding. Subordinates of hydrogen bonding are glimpsed in the protein-ligand binding, which is the backbone donor and acceptor as well as side chain doner acceptor complex of protein 4FRJ & 6ZWE expressed interaction of hydrogen bond with residues of amino acid and for complexes. Scrutinizing the Vander walls radii of 1.4 Å, SASA was computed as median SASA for ligand against target receptor protein (4FRJ & 6ZWE) diminished after binding with complex (Fig. 6).

Succinctness of interaction abides by rGyr; underneath values of rGyr corresponds to higher steadiness and vice versa. The plot of rGyr vs. time of complex BACE1-isorhoifolin & AChE inhibitor-isorhoifolin interposed. Median rGyr for complex BACE1-isorhoifolin and AChE inhibitor-isorhoifolin appeared to be 22 Å² 23.2 Å², respectively, throughout MD simulations run of 200 ns (Fig. 7).

Density functional theory (DFT) studies

It was accomplished to optimize the isorhoifolin structure (Fig. 8A). The discrete atomic bond parameters, such as bond length angle, have been established. The C = O bond length obtained was 1.5 Å, whereas, for the C-H bond, it was 2 Å. To a more significant extent, sites of electrophile nucleophiles were investigated using MEP surface inspection (Fig. 10A). The colour of MEP surfaces (red, yellow, blue, orange, green) indicates charge distribution [24]. The range of charge distribution was − 5.883e-2 to + 5.883e-2. In Fig. 10 (B), the coloured region indicates bulk negative electrostatic potential, whereas the coloured region stipulated the most positive electrostatic potential. A green colour indicates the neutral

electrostatic potential. Oxygen atoms show high electromagnetic potential on MEP surfaces due to their electrophilic reactive nature, whereas carbon atoms show nucleophilic nature [25].

HOMO (Highest Occupied Molecular Orbital) & LUMO (Lowest Unoccupied Molecular Orbital) are merely FMO (Frontier Molecular Orbitals) which are beneficial to recognize numerous chemicals, thermal, and electronic assets of molecules. Energy difference allying HOMO & LUMO of molecules shown by the density of state (DOS), furthermore reactivity of global and local variables was also scrutinizing, for instance, energy aperture, electron energy, chemical solidity as well as downiness, electrophilicity lead intimation, ionization potential [26].

The energy difference between FMO, i.e., and HOMO-LUMO, is -0.162, showing ISF is more reactive. In the structure of ISF, the aromatic ring region appeared to be LUMO surfaces, whereas the aliphatic regions appeared as HOMO regions (Fig. 9). Phytoconstituents expressed equilibrated LUMO energy that fact stipulates ISF exhibit biological solid activity. Those, as mentioned earlier, might be expected because of the existence of a ketonic group. Carbonyl operates as an electron revulsion class. In the report of Koopman's theorem, global local parameters such as LUMO energy characterize a reminiscent part of pharmacological action. Outright hardness with a softness framework can be accustomed to prognosticate phytocompound isorhoifolin excitability and steadiness.

Mulliken occupant's charges, bond length, bond order exploration

Gaussian 6.0.16 software assessed the Mulliken charges, bond length, bond order, etc. These parameters implicate the inclination of ISF phytoconstituents towards the absorption of electrons. The positive charge is exhibited by H and C atoms, whereas oxygen atoms show the negative charge (Fig. 10). Dual descriptors were used to calculate the Fukai function, identifying the difference between electrophile nucleophiles. Higher electrophilic sites stipulate the reactivity of ISF toward biological activity as well as the system.

The following generation of HOMO (-0.2267 ev) and LUMO (-0.06358 ev) and elevated energy gap (-0.162 ev) represent that a high-rise charge transmission takes place with isorhoifolin & creates a steady interaction with target protein concerning to the intensification of the bioactivity (Fig. 10B). The value −0.162 ev stipulates that the molecule has robust inhibition effectiveness due to energy requirement in removing an electron from hindmost molecule inhibitors acquire free electron moreover donate an electron to unoccupied orbital, making them supplemental electron-rich and thus offering supercilious inhibition efficiency. The results showed that isorhoifolin is occupied with electrons since the LUMO value represents a molecule caliber to receive free electrons, supply free electrons, and provide excellent inhibition accomplishment.

ADMET Attributes

The ADMET characteristics of a composite are a predominant feature of its unsympathetic potency. The SwissADME server bestows an adaptable, accessible web frontier to speculate copious ADME parameters [27]. Assimilation of the drugs becomes a restraining facet for their bioavailability and retaliation. A drug is deliberated competently if absorbed in the human intestine exceeding 70% [28]. There is an adaptation of philosophy in the pharmaceutical industry: If a drug fails early, it will fail competitively, which asserts that vigor action, i.e., potency, is not at most property concernment [29]. This emanated in incorporating in-vitro and *in silico*, ADMET parameters at the initial and development stages. Such an approach has the intense possibility of astonishing declination, which is observed in the ADME point at issue seen with the termination of projects [19]. The phytoconstituents of plant *G. asiatica* were analyzed for ADME and toxicity properties the pkcsm server was used for ADME profiling of phytoconstituents with toxicity studies (Table 3).

Computational analysis for drug likeliness with infinitesimal properties sieving

Roughly, drugs are defined as a class of chemically active entities which are having potency, affinity, and intestinal therapeutic efficacy with the target; other than these characteristic properties, they should also fulfill indubitable criteria like bioavailability at the same time devoid of toxicities acute/chronic, any type of carcinogenicity, mutagenicity, genotoxicity, etc. Hence, that objective ADMET framework was enumerated and examined for harmony with their standard compass. A phytoconstituent with high CaCo2 permeability is 0.392, easily absorbed if the Papp coefficient is more than 8×10^{-6}. Besides CaCo2 permeability, if the absorption of the drug is less than 30%, it is a poor candidate for formulation purposes. All the phytoconstituents were anticipated to have sound absorption at the intestine for skin permeability. Log kp values are considered; if it is less than − 2.5, it will have low permeability related to skin [9].

Table 3
ADMET profiling of isorhoifolin.

S. No.	ADMET attributes	Property name (unit)	Speculated values
1	Absorption	Skin permeability (log Kp)	-2.735
		Water solubility (log mol/L)	-3.262
		Caco2 permeability (LOG Papp in 10-6cm/s)	0.392
		P-glycoprotein substrate	Yes
		P-glycoprotein I inhibitor	No
		P-glycoprotein II inhibitor	No
		Intestinal absorption[human](%Absorbed)	30.186
2	Distribution	Fraction unbound [human](Fu)	0.089
		BBB permeability (log BB)	-1.845
		CNS permeability (log PS)	-5.145
		VDss[human] (log L/kg)	0.269
3	Metabolism	CYP2D6 substrate	No
		CYP1A2 inhibitor	No
		CYP3A4 substrate	No
		CYP2C19 inhibitor	No
		CYP2D6 inhibitor	No
		CYP2C9 inhibitor	No
4	Excretion	Renal OCT2 substrate	No
		Total Clearance (log ml/min/kg)	0.451
5	Toxicity	Hepatotoxicity	No
		Skin sensitization	No
		T. Pyriformis toxicity (log ug/L)	0.285
		Minnow toxicity (log mM)	5.005
		Oral rat acute toxicity [LD_{50}] (mol/kg)	3.903
		hERG_ I inhibition	No
		hERG_II inhibition	Yes

Conclusion

Understanding protein-ligand bonding has substantially benefited from arithmetical biology and molecular adaptation. Drug discovery has set off significantly less exorbitant due to the requisition of infinitesimal modeling techniques. The present investigation used phytoconstituents selected from the *G. asiatica* plant. These phytoconstituents were scrutinized for virtual screening using molecular docking and discovered that isorhoifolin was the most interactive and had more affinity energy than other phytoconstituents in the plant. Further study related to docking showed that specific target proteins PDB ID 4FRJ and 6ZWE were potent in terms of binding energy and numerous types of interaction with isorhoifolin. Hence, these complexes of 4FRJ-isorhoifolin and 6ZWE-isorhoifolin were selected for the molecular dynamic simulation study, which runs at 200 ns.

Further MD study revealed that the residues GLY32, TRP36, PRE108, and ARG235 of the 4FRJ-ISF complex and residues THR95, GLU292, and SER293 of the 6ZWE-ISF had hydrogen bond interactions. RMSF, RMSD, and RoG analyses indicate the steady nature of complexes with intimated values. The study expressed that the phytoconstituent isorhoifolin the hit explicated minimal alterations fluctuation in proteins and ligand RMSD, RMSF. Furthermore, isorhoifolin was revolutionized using B3LYP/6-311G (d, p) basis sets by Gaussview 6.0.16 software. The HOMO-LUMO energy gap was examined using an optimized isorhoifolin structure with accompanying orbital energies. From the optimized isorhoifolin structure in the company of B3LYP/6-311G (d, p), MEP surface, bond lengths, Mullikan charge analysis, and bond orders were calculated. Hence, isorhoifolin could be a notable candidate to the greater extent for in-vitro and in-vivo studies, specifically BACE1 targeted proteins as a treatment scheme against AD.

Materials and Methods

Docking studies

Retrieval of proteins and ligands

The *Gmelina asiatica* leaf chemical constituents' data was obtained from the IMMPAT (Indian medicinal plants phytochemistry therapeutics database) database (https://cb.imsc.res.in/imppat/basicse archauth) [30]. The identified phytoconstituents were retrieved from the PubChem database (https://pubchem.ncbi.nlm.nih.gov/). Target proteins BACE1 (PDB: 4FRJ), AChE (PDB: 6ZWE), GSK-3 (PDB: 1Q5K), and TACE (PDB: 2OI0) for Alzheimer's disease with their PDB IDs collected from the RCBS database (https://www.rcsb.org/).

Pre-processing of proteins and ligands

The conversion of the sdf form to the pdb form of all phytoconstituents was done using Pyrex software. Proteins pdb files obtained from the database went through various steps involving the addition of polar hydrogen, merging non-polar hydrogen, adding Colman charges, and removing water molecules and unwanted residues [31]. Followed by assigning an AD4-type radius. These protein pre-processing steps

are done through the auto-dock and discovery studio visualizer software [32]. Conversion of pdb to pdbqt files of target proteins and ligands were done in the auto dock. A grid box was prepared with specific dimensions, as shown in Table 4.

Table 4
Grid dimensions of target proteins

Target protein	X, Y, and Z axis dimensions	Grid box dimensions
AChE (PDB ID:6ZWE)	125.5753 X 27.4496 X -2.9429	72.33 X 56.06 X 64.33
BACE1 (PDB ID: 4FRJ)	35.40 X 46.95 X 84.96	54.63 X 65.39 X 47.26
GSK-3 (PDB ID: 1Q5K)	25.36 X 37 X 8.293	40 X 40 X 40
TACE (PDB ID: 2OI0)	38.697 X 27.474 X 12.571	40 X 40 X 40

Molecular dynamic simulation studies

Target protein-ligand complexes acquired after docking were prone to molecular dynamics simulations maneuvering the Desmond Maestro module. The software illuminates multistorey execution algorithms as its automated hibernation and all the anchor links were used to secure high-speed and unambiguous results. The target protein-ligand docked complex was initially inundated in the TIP3P water model in an orthorhombic configuration. The system was counterpoised by adding two sodium ions at a 0.15M concentration [33]. All the atoms were oriented using refined potentials for fluid simulations using the AA (OPLS-AA) 2005 force field. NVT was accustomed to the orchestra genre with the SHAKE/RATTLE algorithm to curtail the prominence of the covalent cement atoms. The simulations were begun at 300 K and 1 bar pressure for 200 ns [34].

Density functional theory (DFT) studies

The DFT is a widely used computational method for studying molecules' electronic structure and properties. It is an intermediate-level approach that balances accuracy and computational cost, making it a popular choice for many research applications. In the case of compound isorhoifolin, DFT calculations were performed using the B3LYP functional and the 6-311G (d, p) basis set. The B3LYP functional is a widely used hybrid exchange-correlation functional that combines local and non-local exchange and correlation effects [22]. The 6-311G (d, p) basis set is a commonly used basis set that includes additional polarization functions (d and p orbitals) to account for electron correlation effects. The optimization of molecular geometry using DFT calculations can provide important insights into the 3D structure of a molecule, such as Mulliken charges, bond lengths, and bond order.

Abbreviations

AD: Alzheimer's disease, DFT: Density functional theory, HOMO: Highest occupied molecular orbital, LUMO: Lowest occupied molecular orbital, RMSD: Root mean square deviation, RMSF: Root mean square deviation, RG: Radius of gyration, SASA: Solvent accessible surface area, MM-PBSA: Molecular

mechanics Poisson Boltzmann surface area, CYP: Cytochrome P450, Aβ: amyloid-beta, APP: Amyloid processing protein, NFT: Neurofibrillary tangles, GSK-3: Glycogen synthase kinase-3, TACE: TNF-alpha converting enzyme, BACE: enzyme cleaves APP at β-site, IMMPAT: Indian Medicinal Plants, Phytochemistry therapeutics database

Declarations

Conflict of interest

The authors declare no conflict of interest.

Funding statement

This research received no specific grant from funding agencies in the public, commercial, or not-for-profit sectors.

Ethical approval

Not applicable

Acknowledgments

I, Komal Rajesh Andarghiske, thank MHRD, India, and the Indian Institute of Technology (Banaras Hindu University), Varanasi, for providing a fellowship.

Consent for publication

Not applicable

Availability of data and material

Not applicable

References

1. Chen G-f, Xu T-h, Yan Y, Zhou Y-r, Jiang Y, Melcher K, et al. Amyloid beta: structure, biology and structure-based therapeutic development. Acta Pharmacologica Sinica. 2017;38(9):1205-35. doi: 10.1038/aps.2017.28.
2. Du X, Wang X, Geng M. Alzheimer’s disease hypothesis and related therapies. Translational Neurodegeneration. 2018;7(1):2. doi: 10.1186/s40035-018-0107-y.
3. Sadigh-Eteghad S, Sabermarouf B, Majdi A, Talebi M, Farhoudi M, Mahmoudi J. Amyloid-Beta: A Crucial Factor in Alzheimer's Disease. Medical Principles and Practice. 2014;24(1):1-10. doi: 10.1159/000369101.

4. Sadigh-Eteghad S, Sabermarouf B, Majdi A, Talebi M, Farhoudi M, Mahmoudi J. Amyloid-beta: a crucial factor in Alzheimer's disease. Med Princ Pract. 2015;24(1):1-10. doi: 10.1159/000369101.
5. Awasthi M, Singh S, Pandey VP, Dwivedi UN. Alzheimer's disease: An overview of amyloid beta dependent pathogenesis and its therapeutic implications along with in silico approaches emphasizing the role of natural products. Journal of the Neurological Sciences. 2016;361:256-71. doi: https://doi.org/10.1016/j.jns.2016.01.008.
6. Elmaaidomy AH, Abdelmohsen UR, Alsenani F, Aly HF, Eldin Shams SG, Younis EA, et al. The anti-Alzheimer potential of Tamarindus indica: an in vivo investigation supported by in vitro and in silico approaches. RSC Advances. 2022;12(19):11769-85. doi: 10.1039/D2RA01340A.
7. Rahman MS, Zilani MNH, Islam MA, Hasan MM, Islam MM, Yasmin F, et al. In Vivo Neuropharmacological Potential of Gomphandra tetrandra (Wall.) Sleumer and In-Silico Study against β-Amyloid Precursor Protein. Processes. 2021;9(8):1449.
8. Klafki H-W, Staufenbiel M, Kornhuber J, Wiltfang J. Therapeutic approaches to Alzheimer's disease. Brain. 2006;129(11):2840-55. doi: 10.1093/brain/awl280.
9. Khoba K, Kumar S, Chatterjee S, Purty RS. Isolation, Characterization, and In Silico Interaction Studies of Bioactive Compounds from Caesalpinia bonducella with Target Proteins Involved in Alzheimer’s Disease. Applied Biochemistry and Biotechnology. 2023;195(4):2216-34. doi: 10.1007/s12010-022-03937-1.
10. Uddin MJ, Russo D, Rahman MM, Uddin SB, Halim MA, Zidorn C, et al. Anticholinesterase Activity of Eight Medicinal Plant Species: In Vitro and In Silico Studies in the Search for Therapeutic Agents against Alzheimer’s Disease. Evidence-Based Complementary and Alternative Medicine. 2021;2021:9995614. doi: 10.1155/2021/9995614.
11. Mettai M, Daoud I, Mesli F, Kenouche S, Melkemi N, Kherachi R, et al. Molecular docking/dynamics simulations, MEP analysis, bioisosteric replacement and ADME/T prediction for identification of dual targets inhibitors of Parkinson's disease with novel scaffold. In Silico Pharmacol. 2023;11(1):3. doi: 10.1007/s40203-023-00139-3.
12. Martiz RM, Patil SM, Abdulaziz M, Babalghith A, Al-Areefi M, Al-Ghorbani M, et al. Defining the Role of Isoeugenol from Ocimum tenuiflorum against Diabetes Mellitus-Linked Alzheimer’s Disease through Network Pharmacology and Computational Methods. Molecules. 2022;27(8):2398.
13. Singh RH, Narsimhamurthy K, Singh G. Neuronutrient impact of Ayurvedic Rasayana therapy in brain aging. Biogerontology. 2008;9(6):369-74. doi: 10.1007/s10522-008-9185-z.
14. Potshangbam AM, Nandeibam A, Amom T, Potshangbam N, Rahaman H, Rathore RS, et al. An in silico approach to identify potential medicinal plants for treating Alzheimer disease: a case study with acetylcholinesterase. Journal of Biomolecular Structure and Dynamics. 2022;40(4):1521-33. doi: 10.1080/07391102.2020.1828170.
15. Alamro AA, Alsulami EA, Almutlaq M, Alghamedi A, Alokail M, Haq SH. Therapeutic Potential of Vitamin D and Curcumin in an In Vitro Model of Alzheimer Disease. Journal of Central Nervous System Disease. 2020;12:1179573520924311. doi: 10.1177/1179573520924311.

16. Muthukumaran U, Govindarajan M, Rajeswary M, Hoti SL. Synthesis and characterization of silver nanoparticles using Gmelina asiatica leaf extract against filariasis, dengue, and malaria vector mosquitoes. Parasitology Research. 2015;114(5):1817-27. doi: 10.1007/s00436-015-4368-4.
17. Vasudev P, Shreedhara C, Chandrashekar K, Yamini D. Neuroprotective action of Gmelina arborea (bark) and Punica granatum (peel) extracts. Asian J Pharm https://doi org/101016/j ajps. 2015;4.
18. Kumar S, Chowdhury S, Kumar S. In silico repurposing of antipsychotic drugs for Alzheimer's disease. BMC Neuroscience. 2017;18(1):76. doi: 10.1186/s12868-017-0394-8.
19. Khare N, Maheshwari SK, Jha AK. Screening and identification of secondary metabolites in the bark of Bauhinia variegata to treat Alzheimer's disease by using molecular docking and molecular dynamics simulations. Journal of Biomolecular Structure and Dynamics. 2021;39(16):5988-98. doi: 10.1080/07391102.2020.1796798.
20. Thakur A, Sharma B, Parashar A, Sharma V, Kumar A, Mehta V. 2D-QSAR, molecular docking and MD simulation based virtual screening of the herbal molecules against Alzheimer's disorder: an approach to predict CNS activity. Journal of Biomolecular Structure and Dynamics.1-15. doi: 10.1080/07391102.2023.2192805.
21. Bhanukiran K, T.A G, Krishnamurthy S, Singh SK, Hemalatha S. Discovery of multi-target directed 3-OH pyrrolidine derivatives through a semisynthetic approach from alkaloid vasicine for the treatment of Alzheimer's disease. European Journal of Medicinal Chemistry. 2023;249:115145. doi: https://doi.org/10.1016/j.ejmech.2023.115145.
22. Bhanukiran K, Singh R, T A G, Ramakrishna K, Singh SK, Krishnamurthy S, et al. Vasicinone, a pyrroloquinazoline alkaloid from Adhatoda vasica Nees enhances memory and cognition by inhibiting cholinesterases in Alzheimer's disease. Phytomedicine Plus. 2023;3(2):100439. doi: https://doi.org/10.1016/j.phyplu.2023.100439.
23. Swetha R, Sharma A, Singh R, Ganeshpurkar A, Kumar D, Kumar A, et al. Combined ligand-based and structure-based design of PDE 9A inhibitors against Alzheimer's disease. Molecular Diversity. 2022;26(5):2877-92. doi: 10.1007/s11030-022-10504-7.
24. Ngo ST, Li MS. Top-leads from natural products for treatment of Alzheimer's disease: docking and molecular dynamics study. Molecular Simulation. 2013;39(4):279-91. doi: 10.1080/08927022.2012.718769.
25. Bhanukiran K, Singh SK, Singh R, Kumar A, Hemalatha S. Discovery of Multitarget-Directed Ligands from Piperidine Alkaloid Piperine as a Cap Group for the Management of Alzheimer's Disease. ACS Chemical Neuroscience. 2023. doi: 10.1021/acschemneuro.3c00269.
26. Gnanaraj C, Sekar M, Fuloria S, Swain SS, Gan SH, Chidambaram K, et al. In Silico Molecular Docking Analysis of Karanjin against Alzheimer’s and Parkinson’s Diseases as a Potential Natural Lead Molecule for New Drug Design, Development and Therapy. Molecules. 2022;27(9):2834.
27. Amat-ur-Rasool H, Ahmed M. Designing Second Generation Anti-Alzheimer Compounds as Inhibitors of Human Acetylcholinesterase: Computational Screening of Synthetic Molecules and Dietary

Phytochemicals. PLOS ONE. 2015;10(9):e0136509. doi: 10.1371/journal.pone.0136509.

28. Abraham JT, Maharifa HNS, Hemalatha S. In Silico Molecular Docking Approach Against Enzymes Causing Alzheimer’s Disease Using Borassus flabellifer Linn. Applied Biochemistry and Biotechnology. 2022;194(4):1804-13. doi: 10.1007/s12010-021-03779-3.
29. Raffa DF, Rauk A. Molecular Dynamics Study of the Beta Amyloid Peptide of Alzheimer's Disease and Its Divalent Copper Complexes. The Journal of Physical Chemistry B. 2007;111(14):3789-99. doi: 10.1021/jp0689621.
30. Chlebek J, Korábečný J, Doležal R, Štěpánková Š, Pérez DI, Hošťálková A, et al. In Vitro and In Silico Acetylcholinesterase Inhibitory Activity of Thalictricavine and Canadine and Their Predicted Penetration across the Blood-Brain Barrier. Molecules. 2019;24(7). doi: 10.3390/molecules24071340.
31. Basu A, Sarkar A, Maulik U. Molecular docking study of potential phytochemicals and their effects on the complex of SARS-CoV2 spike protein and human ACE2. Scientific Reports. 2020;10(1):17699. doi: 10.1038/s41598-020-74715-4.
32. Garg S, Anand A, Lamba Y, Roy A. Molecular docking analysis of selected phytochemicals against SARS-CoV-2 Mpro receptor. Vegetos. 2020;33(4):766-81. doi: 10.1007/s42535-020-00162-1.
33. Seniya C, Khan GJ, Uchadia K. Identification of Potential Herbal Inhibitor of Acetylcholinesterase Associated Alzheimer’s Disorders Using Molecular Docking and Molecular Dynamics Simulation. Biochemistry Research International. 2014;2014:705451. doi: 10.1155/2014/705451.
34. Akawa OB, Subair TI, Soremekun OS, Olotu FA, Soliman MES. Structural alterations in the catalytic core of hSIRT2 enzyme predict therapeutic benefits of Garcinia mangostana derivatives in Alzheimer's disease: molecular dynamics simulation study. RSC Advances. 2021;11(14):8003-18. doi: 10.1039/D0RA10459K.

Figures

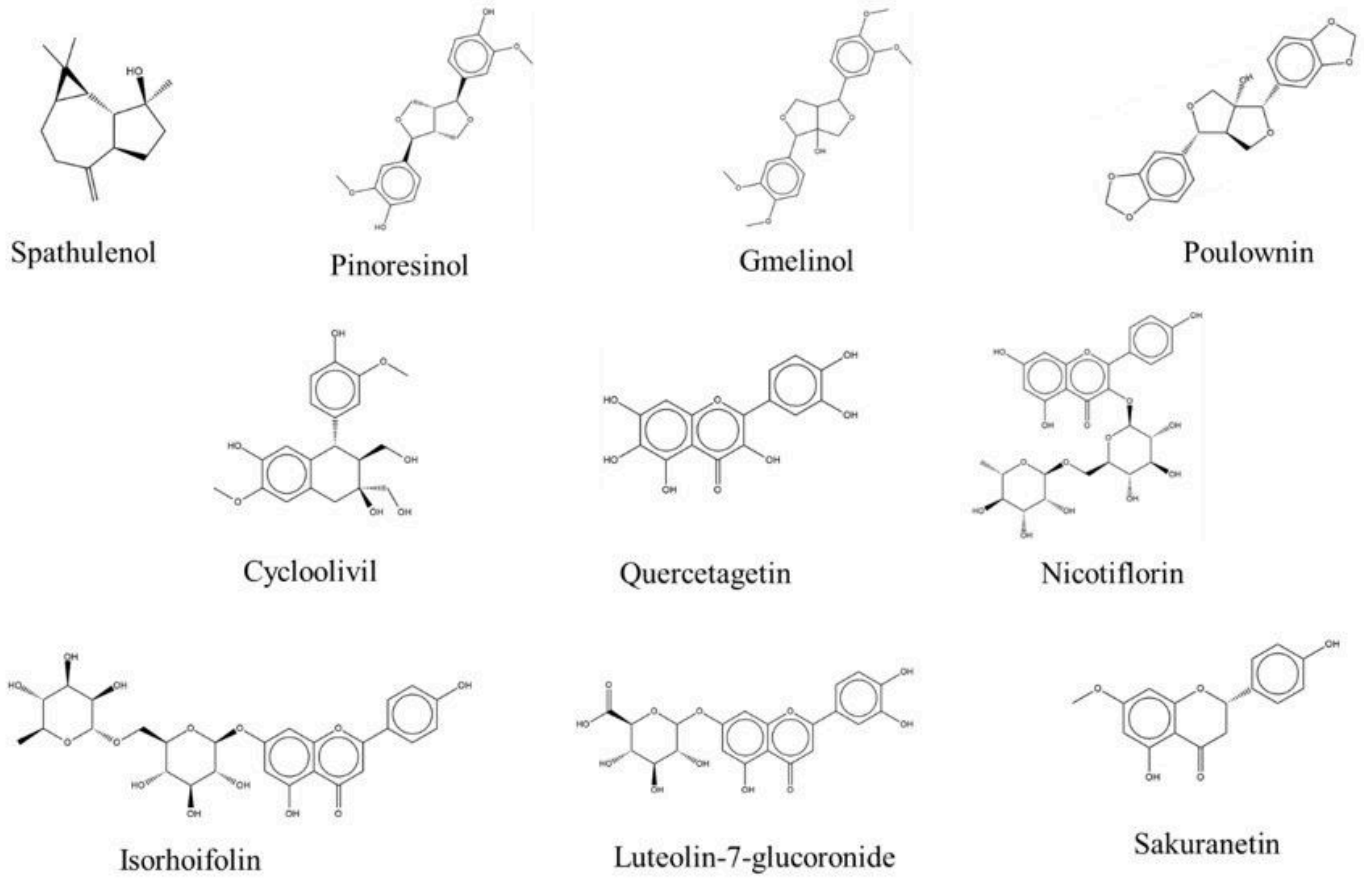

Figure 1

Structures of phytoconstituents from *Gmnelia asiatica*

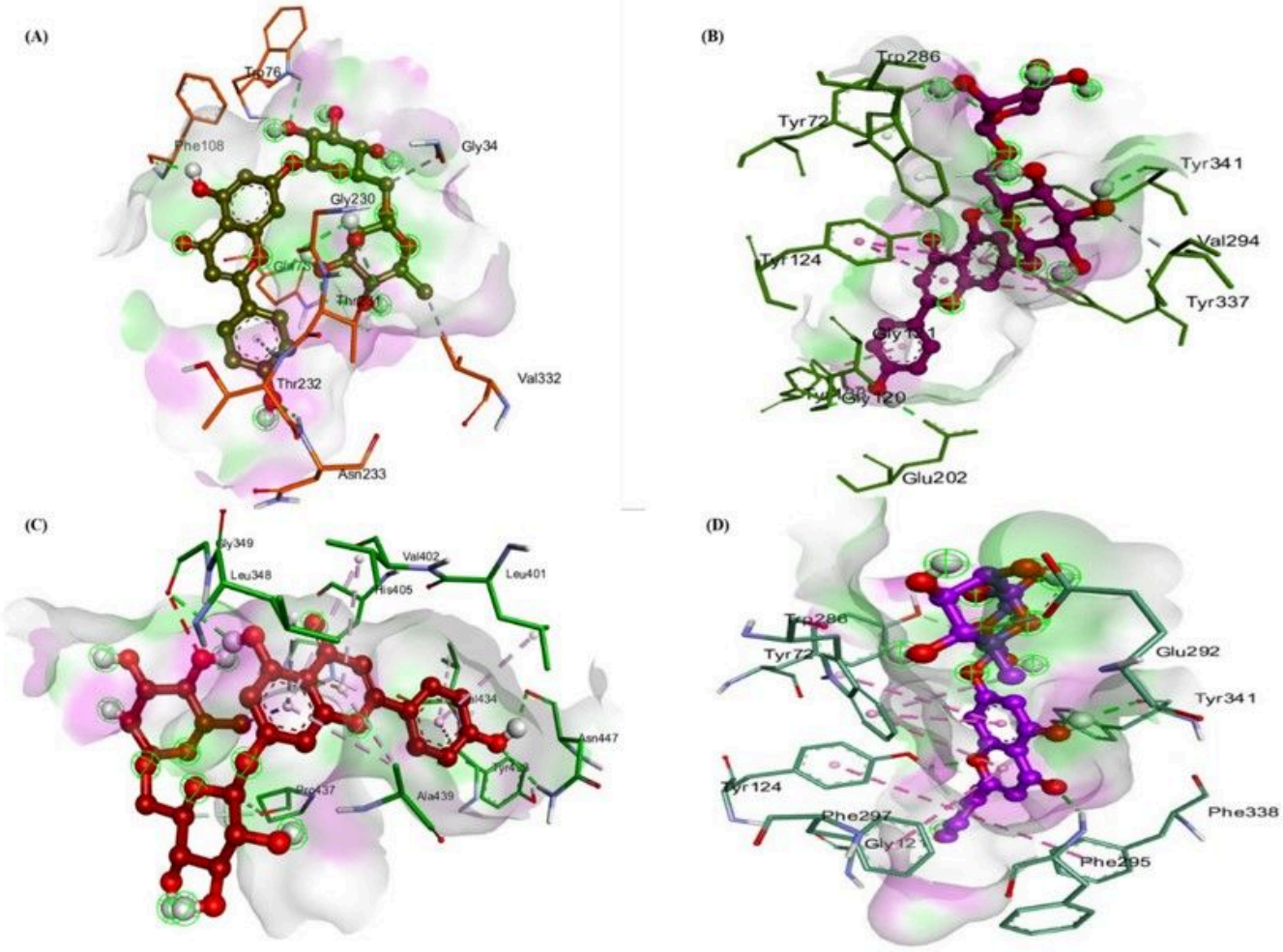

Figure 2

(A), (B), (C) & (D) 3D diagram of BACE1-isorhoifolin, AChE inhibitor-isorhoifolin, TNF3-isorhoifolin, and GSK3-isorhoifolin respectively.

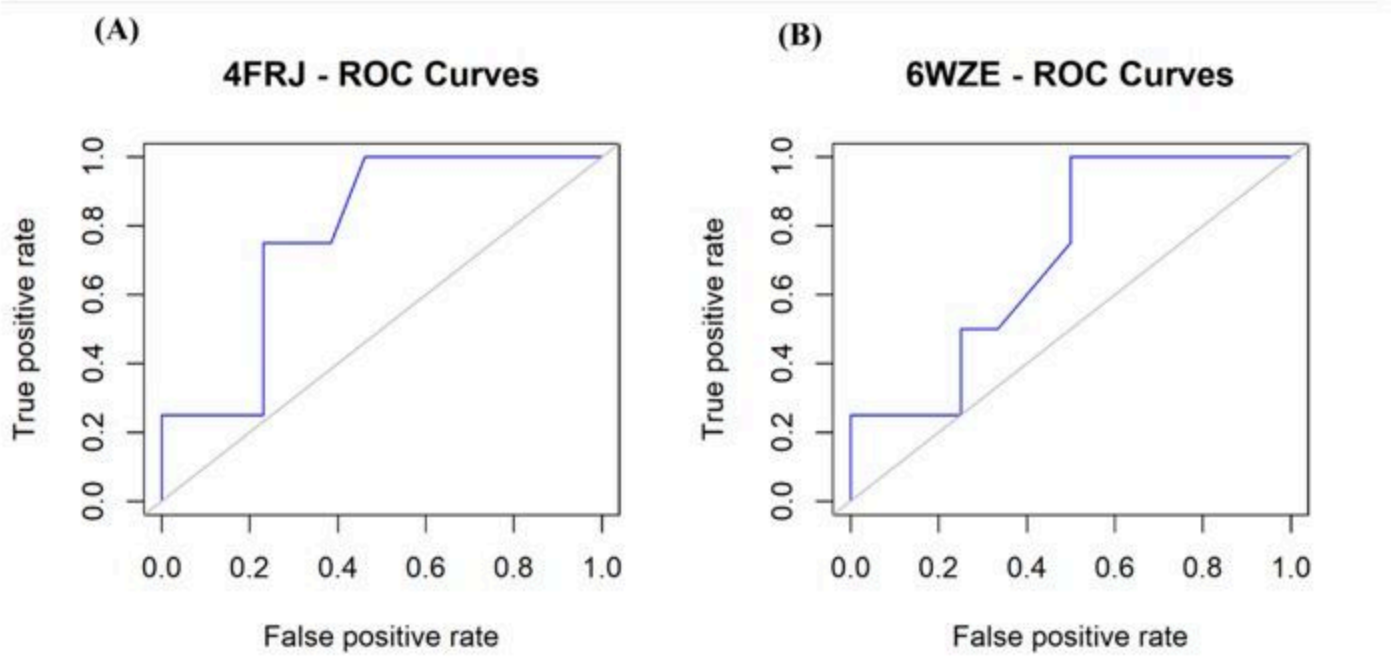

Figure 3

(A) & (B) ROC curves of docked complexed proteins 4FRJ & 6ZWE with isorhoifolin

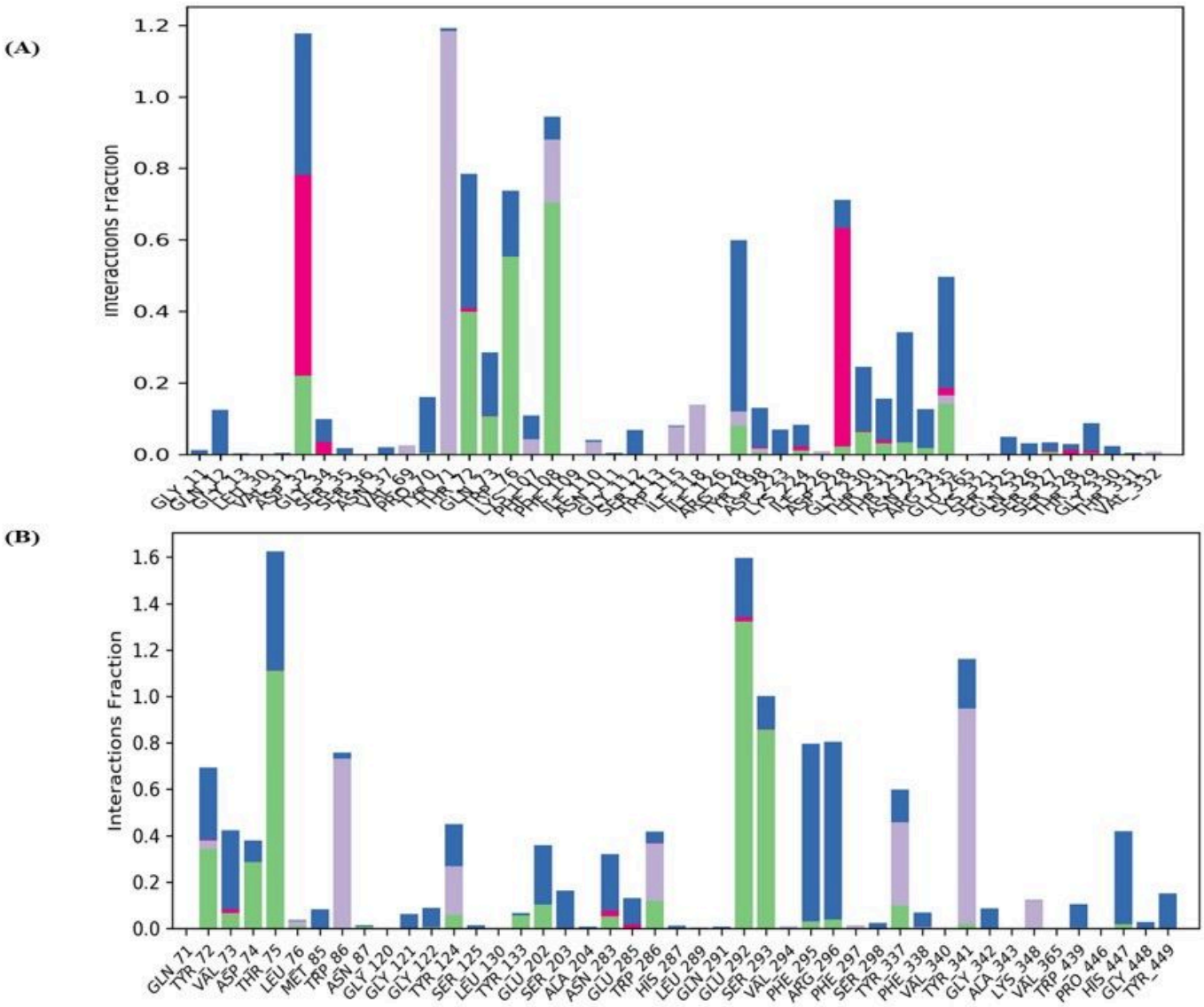

Figure 4

(A), (B) Types of bond interaction of target protein complexes 4FRJ-isorhoifolin (BACE1) & 6ZWE-isorhoifolin (AChE), respectively.

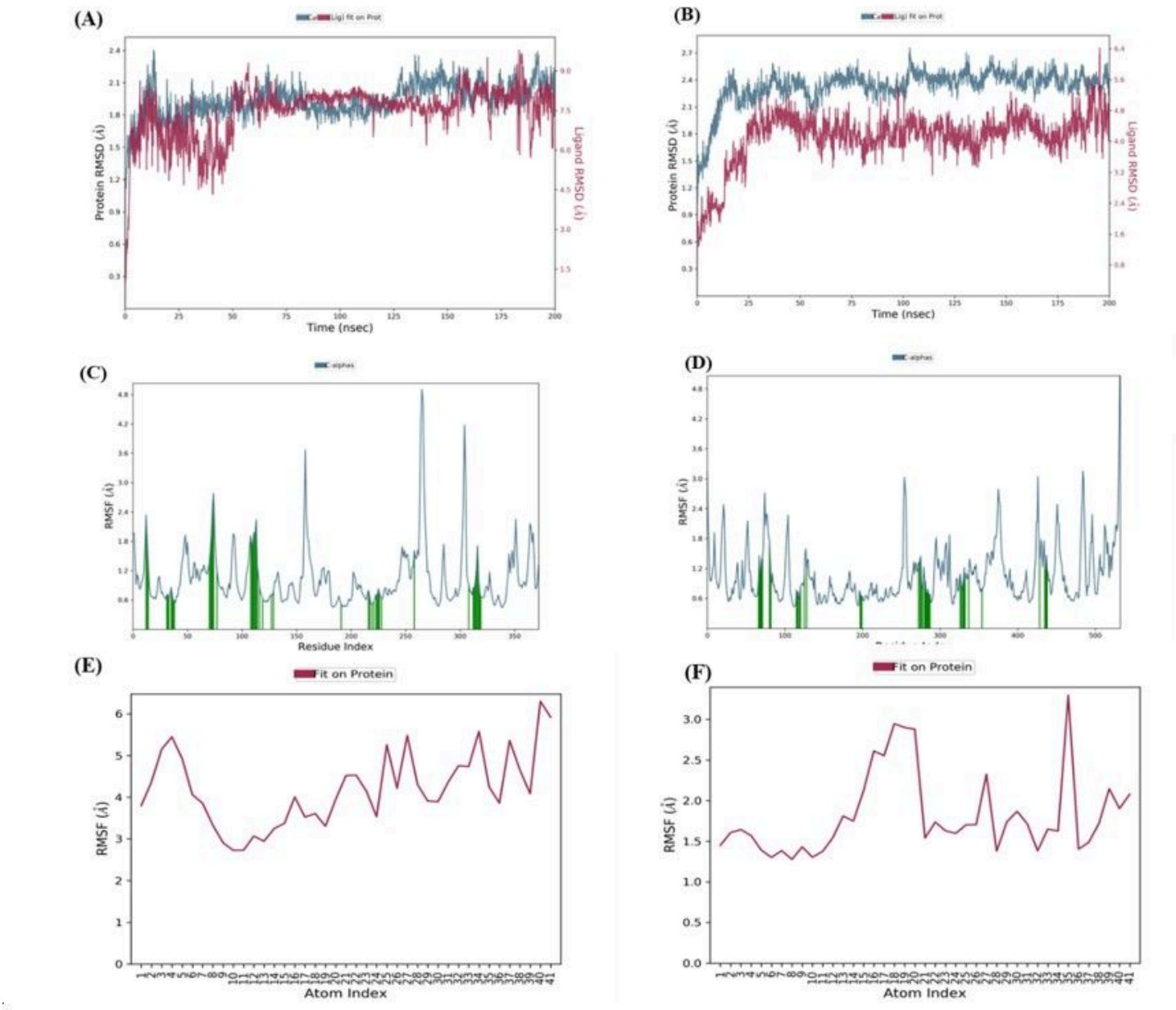

Figure 5

(A) & (B) protein BACE1& AChE inhibitor RMSD with ligand isorhoifolin RMSD plot, (C) & (D) protein 4FRJ, 6ZWE RMSF plot, (E) & (F) ligand isorhoifolin RMSF plot.

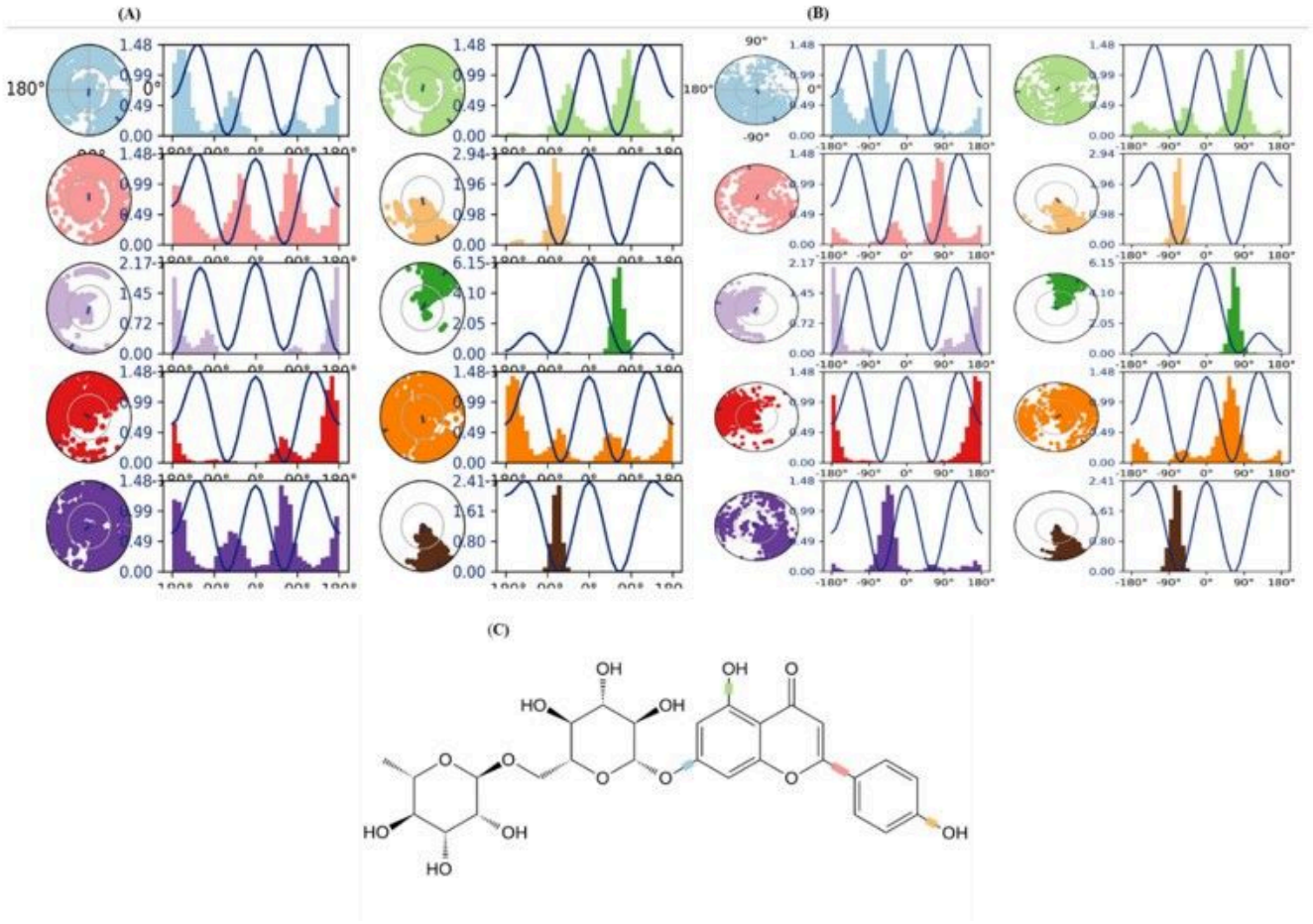

Figure 6

(A), (B), & (C) Isorhoifolin torsion profile concerning complex of protein 4FRJ & 6ZWE, respectively.

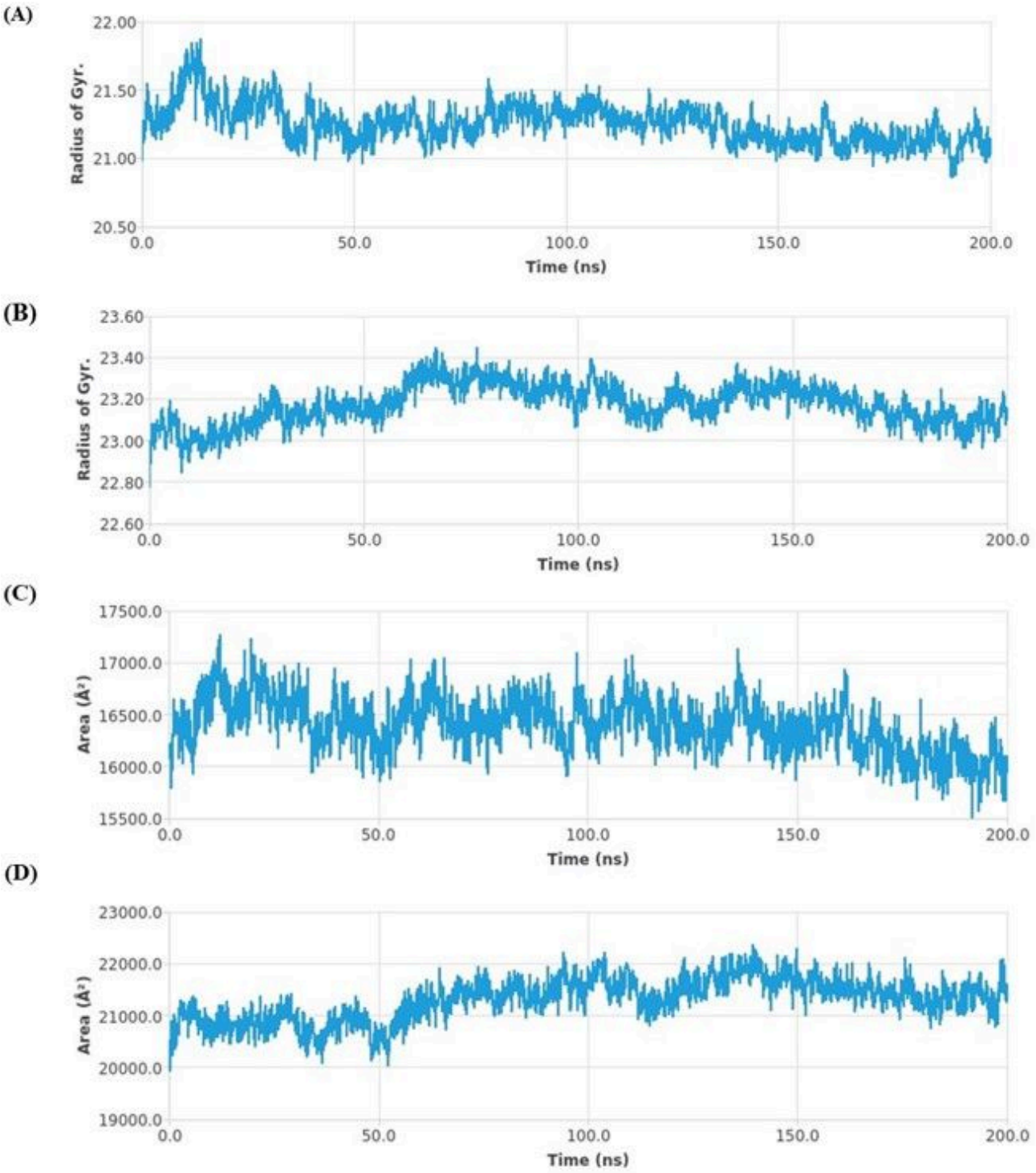

Figure 7

(A), (B), (C) & (D) Radius of gyration and SASA plot of target protein BACE1& AChE inhibitor with isorhoifolin complex, respectively.

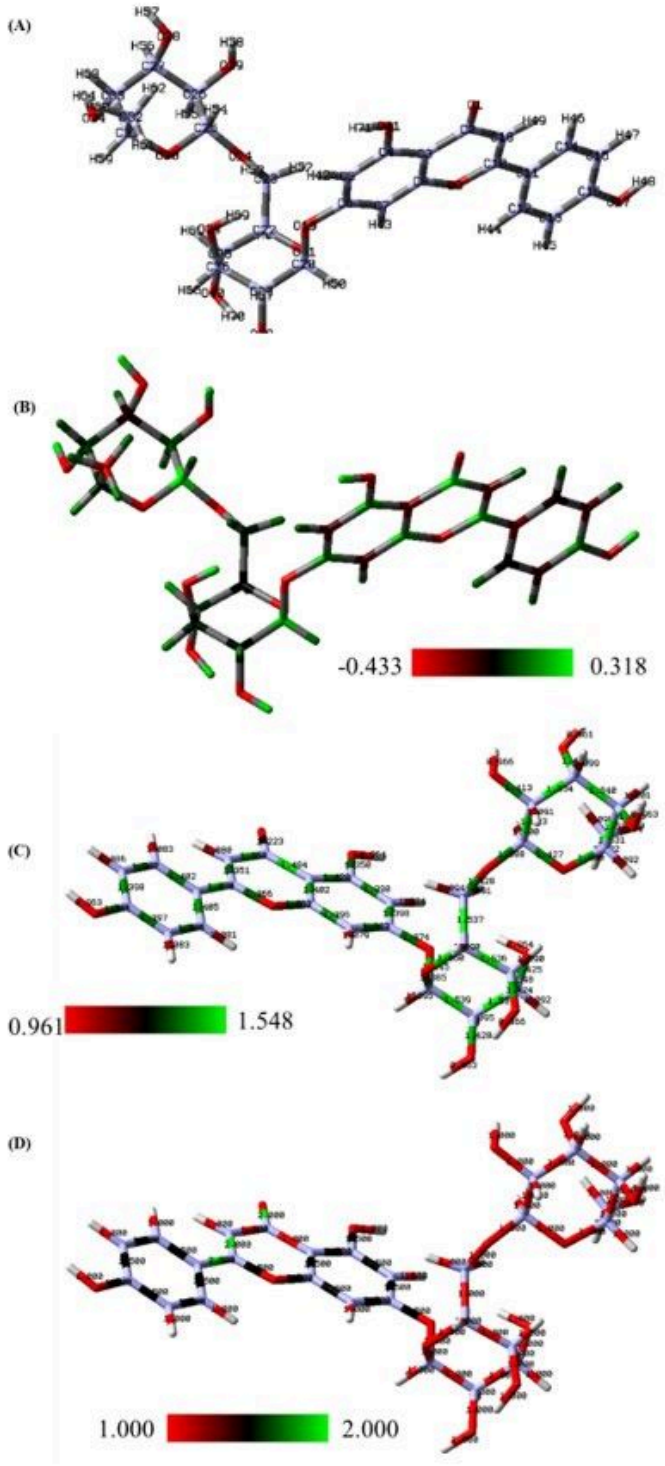

Figure 8

(A) Numbered structure of isorhoifolin, **(B)** Colour-charged representation of isorhoifolin**. (C) & (D)** Bond length & bond order values illustration of atoms of isorhoifolin.

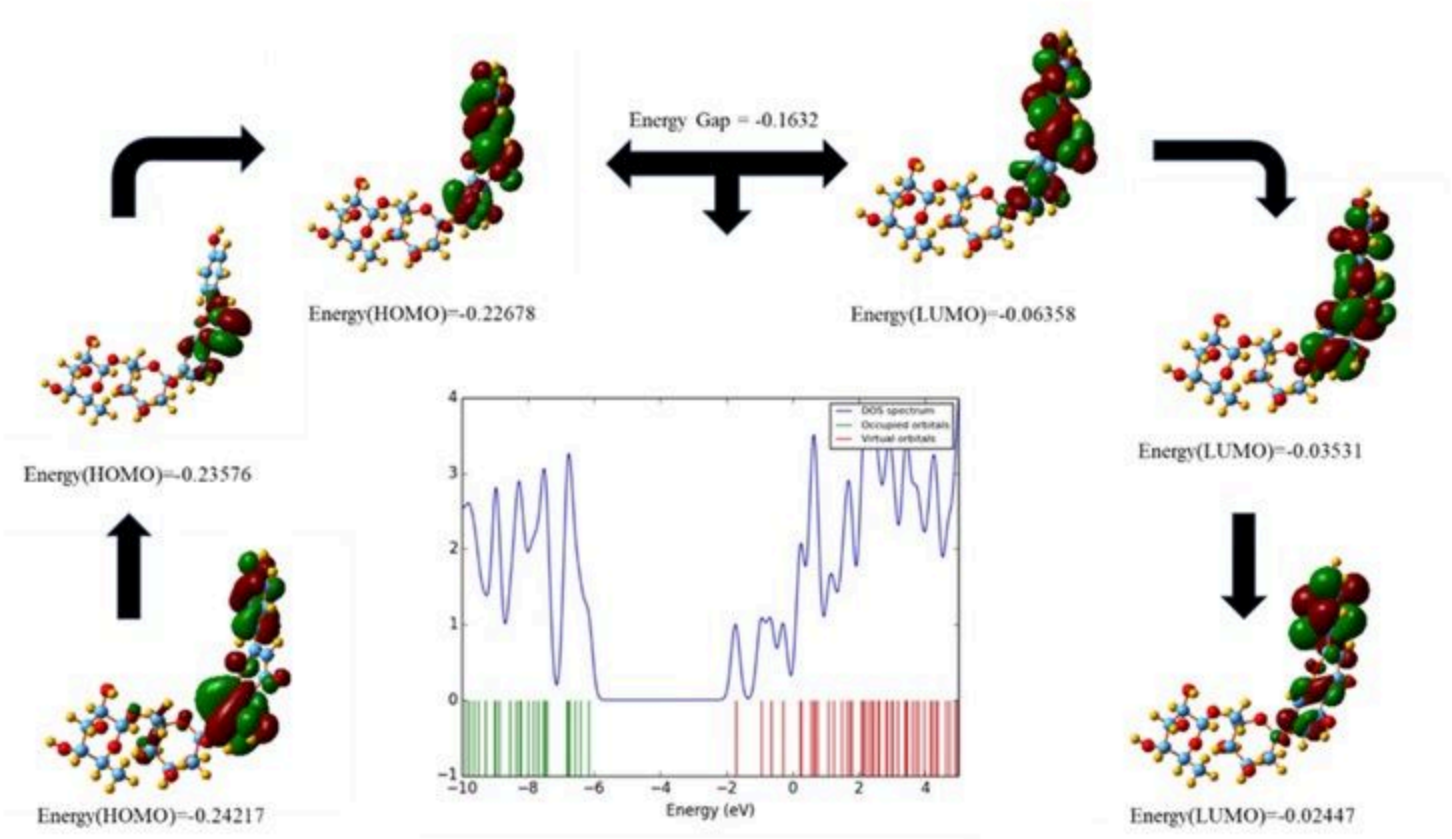

Figure 9

HOMO-LUMO energy split and DOS spectra of isorhoifolin.

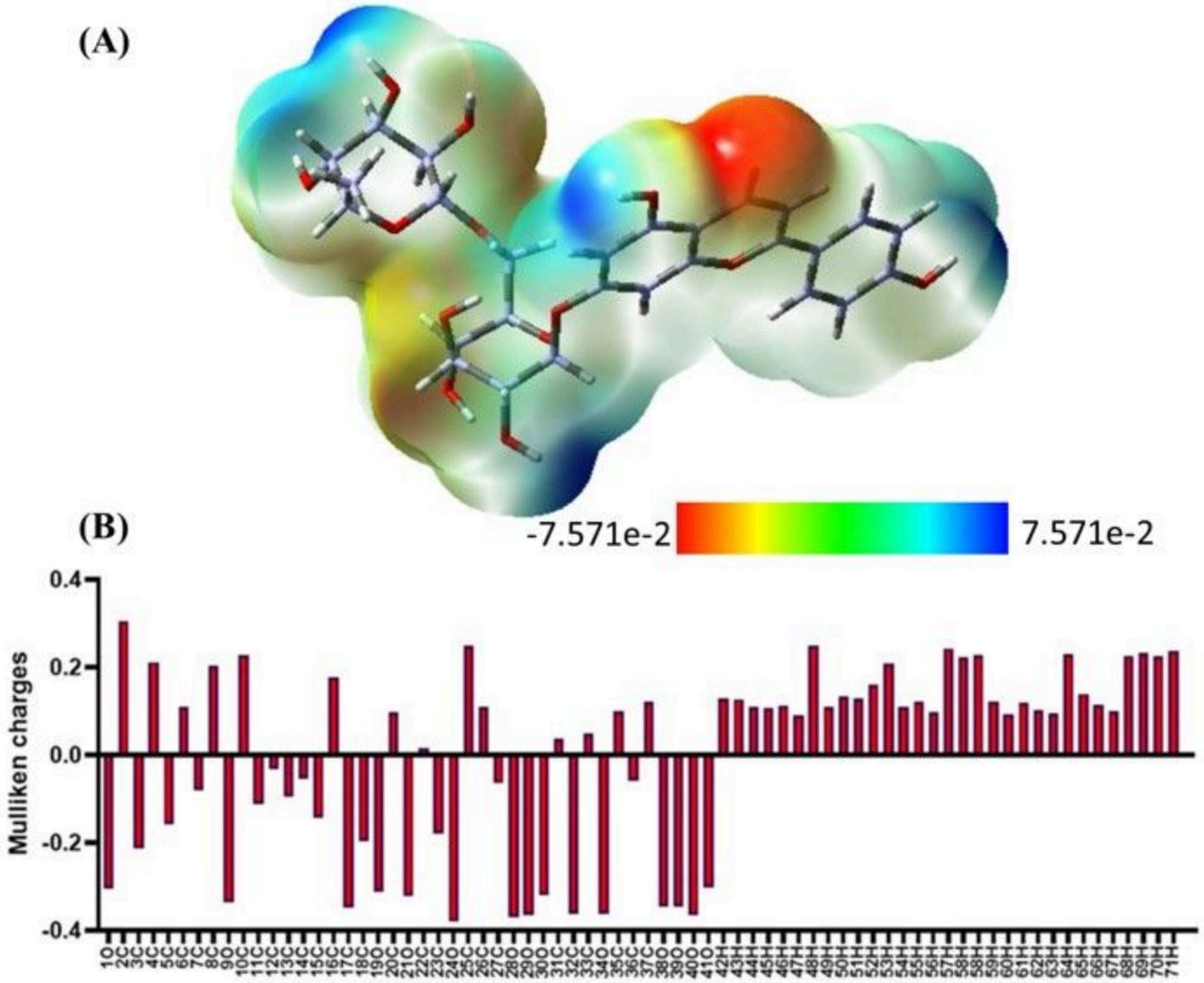

Figure 10

(A) Molecular electrostatic potential (MEP) surface of isorhoifolin. **(B)** Illustration showing mulliken charges of each atom of isorhoifolin.

Supplementary Files

This is a list of supplementary files associated with this preprint. Click to download.

- GraphicalAbstract.jpg